

Completeness Assessment and Autonomous Resampling of Building Point Clouds with Aerial Priors

Yujie Chen¹, Shengjun Tang^{1,*}, Weixi Wang¹, Tian Yu¹, Linfu Xie¹, Xiaoming Li¹,
Yunjie Zhang², Renzhong Guo¹

¹ School of Architecture and Urban Planning, Shenzhen University, Shenzhen, P.R. China -
15197186100@163.com, 15197186100@163.com, (shengjuntang,wangwx,linfuxie,lxm,guorz)@szu.edu.cn

² School of Intelligent Systems Engineering, Sun Yat-sen University, Shenzhen, P.R. China -
zhangyj386@mail.sysu.edu.cn

KEY WORDS: Completeness Assessment, Building Modeling, Point Cloud, 3D Scene

ABSTRACT:

Based on methods such as airborne oblique photogrammetry and laser scanning, high-precision urban 3D point clouds can be obtained. However, existing airborne 3D data acquisition techniques are prone to interference from dense building occlusions or vegetation cover, making it difficult to capture complete building point clouds. To address this issue, this paper proposes a sky-ground cross-perspective collaborative method for building point cloud completeness detection and autonomous completion. The core idea of this method is to use aerial point clouds as a basis, conducting completeness detection of airborne building point clouds to identify missing regions in both point and surface forms. Subsequently, aerial point cloud priors are employed to guide global and local route planning for ground platforms. Finally, an autonomous completion of building point clouds is achieved through a multi-objective TARE exploration method. The proposed method is evaluated through experiments conducted in both simulation and real-world scenarios. Effectiveness analysis is performed from the perspectives of point cloud completeness and building model reconstruction accuracy. The results show that the proposed sky-ground cross-perspective collaborative point cloud completion method can acquire building point clouds with higher completeness and significantly improve the modeling accuracy of building point clouds.

1. INTRODUCTION

Three-dimensional building models are essential for various applications, including urban planning (Cao et al., 2021, Fidan et al., 2023), smart cities (Jovanović et al., 2020, Sariturk et al., 2023), autonomous driving, and low-altitude unmanned systems (Maboudi et al., 2023). Accurate 3D reconstruction from point clouds or images has become a significant research area in photogrammetry and computer vision (Yu et al., 2021, Li and Shan, 2022). Traditionally, airborne LiDAR and oblique photogrammetry are used to acquire point clouds of urban buildings (Wu et al., 2023), but these methods often encounter challenges in dense urban environments, where factors such as vegetation, hollow building bases, and occlusions prevent the full acquisition of building facades and bases (Fruh and Zakhor, 2003, Liu et al., 2024a, Li et al., 2025). These gaps in data lead to significant reductions in reconstruction accuracy (Elhashash and Qin, 2022, Forster et al., 2013).

A promising solution to overcome these challenges is cross-view collaborative surveying, which combines aerial and ground perspectives to acquire comprehensive building point clouds, enabling accurate 3D model reconstruction (Liu et al., 2024b, Huang et al., 2017, Ma et al., 2023). Existing research has primarily focused on cross-view point cloud registration and collaborative localization between aerial and ground platforms (Elhashash and Qin, 2022, Ling and Qin, 2022, Zhou et al., 2023). These approaches typically address the alignment of point clouds from different perspectives, using methods such as feature point matching to estimate rotation and translation (Lee et al., 2024, Persad and Armenakis, 2017). However, most studies have concentrated on improving localization and registration, with less emphasis on optimizing the acquisition of missing data or minimizing redundancy during data collection.

Several methods have been proposed to fuse data from aerial and ground platforms for more complete point clouds. Some studies have used aerial data as a con-

* Corresponding author

straint to assist ground-based localization and mapping (Elhashash and Qin, 2022, Potena et al., 2019), but these methods focus more on improving trajectory tracking and localization rather than ensuring the completeness of the data. Additionally, some methods, such as (Sun et al., 2023), use aerial data for object geo-localization to enhance the accuracy of ground-based systems, yet they do not tackle the problem of filling in missing data. Other methods, like (Miller et al., 2022), propose joint mapping between aerial and ground platforms, but fail to address the automation of data collection for missing point clouds. Moreover, ground-based data collection remains highly manual and prone to inefficiencies, resulting in redundant data and high costs.

While the integration of aerial and ground-based systems has made significant advances, a gap remains in the automated detection of missing data and the generation of efficient collaborative acquisition routes. The current solutions often fall short of providing a comprehensive approach for optimizing data acquisition and ensuring completeness in dense urban environments. In response to these challenges, we propose a novel cross-view collaborative surveying method that leverages aerial point cloud data to automatically detect missing areas and generate optimized acquisition paths for ground-based systems. Our method enhances the accuracy and efficiency of data collection by systematically identifying regions with missing data and planning autonomous data acquisition routes for these areas. This approach not only reduces redundancy in data collection but also ensures comprehensive point cloud coverage for 3D building reconstruction. The main contributions of our work are as follows: 1) A cross-view collaborative surveying framework for 3D building reconstruction that integrates aerial and ground data with automatic path planning; 2) An innovative building integrity detection algorithm based on multi-layer slice projections for identifying regions with missing data; and 3) An automated method for generating ground-based acquisition routes, combining global path planning and autonomous exploration techniques to optimize data collection.

2. METHODOLOGY

2.1 Overview

To overcome these limitations on complete collection of building point cloud, this paper introduces an innovative sky-ground cross-perspective collaborative method for building point cloud completeness detection and autonomous completion shown in Figure 1. The central premise of this method is to leverage aerial point

clouds as a foundational reference. By performing completeness detection on airborne building point clouds, the algorithm can identify regions that are missing both in terms of individual points and surface structures. This process allows for the systematic identification of gaps caused by occlusions or other obstructions during data acquisition. Once the missing regions are identified, aerial point cloud priors are utilized to guide both global and local route planning for ground-based platforms, such as autonomous vehicles or drones. This collaborative approach ensures that the ground platforms are directed to the most crucial areas where data acquisition is lacking, improving the efficiency and accuracy of subsequent point cloud collection. The integration of aerial and ground-based perspectives also allows for continuous real-time adjustment of the collection strategy, optimizing the overall process. Finally, the method incorporates a multi-objective TARE (Targeted Autonomous Resampling Exploration) approach to autonomously complete the building point clouds. This technique not only aims to fill in the missing regions but also ensures that the completed point clouds meet the desired quality standards, balancing both spatial coverage and geometric accuracy.

2.2 3D Scene Classification and Segmentation

This work performs semantic segmentation of 3D point clouds, classifying points into three categories: ground, vegetation, and buildings. A Random Forest (RF) classifier is trained using geometric, intensity, and contextual features, including point density (ρ), height above ground (z), and curvature (σ). The RF model consists of decision trees that split data based on thresholds minimizing Gini impurity, which is computed as:

$$Gini(D) = 1 - \sum_c P_c^2, \quad (1)$$

where P_c is the proportion of points in class c within data subset D . During inference, each point is classified based on majority voting across all trees. The model is trained using a labeled dataset, and its performance is evaluated using precision, recall, F1-score, and confusion matrices.

After semantic segmentation, the building points are further individualized using 2D building footprints. The building-classified points are projected onto the horizontal plane by retaining only the x and y coordinates, which simplifies the spatial relationship between points and 2D building footprints:

$$\mathbf{q}_i = [x_i, y_i], \quad (2)$$

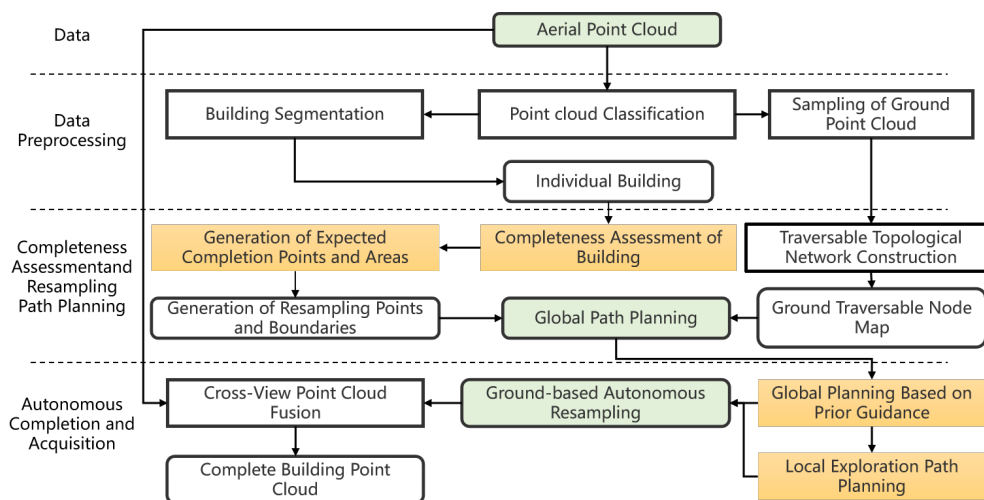


Figure 1. Overview of our proposed framework.

A point-in-polygon test is used to identify points inside the building boundaries, defined as:

$$\mathcal{P}_j = \{\mathbf{p}_i \in \mathcal{P}_b \mid \mathbf{q}_i \in \mathcal{F}_j\}, \quad (3)$$

where \mathcal{P}_b is the set of building-classified points and \mathcal{F}_j represents the j -th building footprint. This process segments the point cloud into individual buildings, enabling further analysis and applications in urban environments.

2.3 Building Integrity Detection Algorithm Based on Multi-Layer Slice Projection

This paper proposes a building point cloud integrity detection algorithm based on multi-layer slice projection to identify missing regions in airborne building point cloud data. The method is designed for both single and complex building structures, with the latter consisting of a podium and multiple individual structures. First, the building point cloud is sliced at various elevation levels, and the sliced point clouds are projected onto the 2D plane to extract contours. The building's 2D contour is obtained by projecting the entire point cloud onto the xy -plane:

$$\mathcal{C}_{building} = \{(x_i, y_i) \mid (x_i, y_i, z_i) \in \mathcal{P}\}. \quad (4)$$

For complex buildings, clustering algorithms are applied to the contours to distinguish the projections of

individual structures. Medial axis transformation is applied to the contours of single structures to compute their skeleton points, denoted as $\mathcal{S}_{k,j} = \{\mathbf{s}_m \mid m = 1, 2, \dots, M_{k,j}\}$. Each boundary point is connected to the nearest skeleton point, and if the contour points of the sliced cloud do not intersect this line, they are labeled as uncollected; otherwise, they are classified as collected.

To identify missing regions, the algorithm computes the shortest distance from each point $\mathbf{p}_i \in \mathcal{C}_{k,j}$ to the line segment connecting the skeleton points \mathbf{s}_m and global contour points $\mathbf{q}_n \in \mathcal{C}_{building}$:

$$d(\mathbf{p}_i, \overline{\mathbf{s}_m \mathbf{q}_n}), \quad (5)$$

where the point \mathbf{p}_i is classified as a missing point if the distance exceeds a threshold δ , otherwise, it is labeled as collected. This process is applied iteratively across all skeleton points and contours, enabling comprehensive detection of missing regions within the building's point cloud.

2.4 Automatic Calculation of Point-Based and Regional-Based Ground Data Supplementation

This study proposes a method for determining the appropriate ground data supplementation strategy based on the ratio of missing points to the total boundary points in building contours. The supplementation strategies are categorized into point-based supplementation for minimal missing regions and regional-based supplementation for larger missing regions. For point-based

supplementation, skeleton points are connected to missing boundary points, and extension lines are drawn outward. Supplemental coordinate points are sampled along these extensions, followed by downsampling to produce the final target points. Mathematically, for each missing point m_i , the Euclidean distance to the nearest boundary point $q_{nearest}$ is computed:

$$d_{im} = \|m_i - s_m\|_2 = \sqrt{(m_{i_x} - s_{m_x})^2 + (m_{i_y} - s_{m_y})^2}, \quad (6)$$

where m_{i_x}, m_{i_y} are the coordinates of the missing point m_i and s_{m_x}, s_{m_y} are those of the nearest skeleton point s_m . For regional-based supplementation, a buffer region is calculated around the missing contour, and the region is expanded outward, defining the supplementation area. The method efficiently handles both types of supplementation, improving the precision of ground-based data collection.

To determine the appropriate supplementation method, the ratio of missing boundary points $R_{missing}$ to the total boundary points is calculated:

$$R_{missing} = \frac{|C_{B,missing}|}{|C_{Building}|}, \quad (7)$$

where $C_{B,missing}$ denotes the set of missing boundary points, and $C_{Building}$ is the total set of building boundary points. If $R_{missing} < \theta$, point-based supplementation is applied; otherwise, regional-based supplementation is used. For point-based supplementation, a ray is cast from each missing boundary point towards the nearest skeleton point, with sampled target points generated along the ray. The final target points are down-sampled:

$$\mathcal{T}_{down} = \mathcal{D}(\mathcal{T}), \quad (8)$$

where \mathcal{T} represents the set of sampled target points, and \mathcal{T}_{down} is the down-sampled set. For regional-based supplementation, the boundary points are expanded outward along their normal vectors, and the convex hull of the expanded points defines the region requiring completion:

$$\mathcal{R}_{complete} = \mathcal{H}(\mathcal{B}_{expand}), \quad (9)$$

where \mathcal{H} denotes the convex hull operation applied to the expanded boundary points.

2.5 Path Planning for Automated Point Cloud Supplementation

This study introduces a path planning method for automated point cloud supplementation by constructing a ground topology graph. First, an airborne 3D point cloud dataset is processed to extract ground points using the Cloth Simulation Filter (CSF) algorithm (Zhang et al., 2016), resulting in a filtered ground point cloud \mathcal{P}_{ground} . A distance-based downsampling method is then applied to produce a set of ground nodes $\mathcal{V}_{ground} = \{\mathbf{v}_1, \dots, \mathbf{v}_N\}$. The pairwise Euclidean distance between nodes is computed, and a connection is established if the distance $d_{\mathbf{v}_i\mathbf{v}_j} = \|\mathbf{v}_i - \mathbf{v}_j\|_2$ is below a threshold $d_{threshold}$. A collision check is performed using the non-ground point cloud $\mathcal{P}_{non-ground}$ to refine the graph by removing edges that intersect non-ground points, resulting in the final ground topology graph $\mathcal{G}_{ground} = (\mathcal{V}_{ground}, \mathcal{E}_{ground})$.

For path planning, the target points $\mathcal{T}_{down} = \{\mathbf{t}_1, \dots, \mathbf{t}_L\}$ and target regions $\mathcal{B}_{expand} = \{\mathbf{b}_i^{expand} \mid i = 1, \dots, N\}$ are integrated into the ground topology graph. For each target point \mathbf{t}_i , the nearest ground node $\mathbf{v}_{nearest}$ is found by minimizing the Euclidean distance:

$$\mathbf{v}_{nearest} = \arg \min_{\mathbf{v} \in \mathcal{V}_{ground}} \|\mathbf{v} - \mathbf{t}_i\|_2. \quad (10)$$

For each target region \mathbf{b}_j^{expand} , the intersection with ground nodes is computed and marked as region-specific candidate nodes. The final traversal set, $\mathcal{V}_{traverse}$, is the union of point- and region-specific nodes:

$$\mathcal{V}_{traverse} = \mathcal{V}_{traverse}^{point} \cup \mathcal{V}_{traverse}^{region}. \quad (11)$$

A distance matrix D shown in Table 1 is constructed to capture topological distances between all candidate nodes, including point-to-point, point-to-region, and region-to-region distances. The shortest distance between candidate nodes is used to generate an efficient path. The global traversal path is initialized from the starting point, and the algorithm alternates between visiting point-specific and region-specific nodes, using the shortest distance matrix to guide the path. Local exploration paths are activated for regions, ensuring full coverage while minimizing traversal length. This approach integrates global and local paths for efficient automated data supplementation.

	\mathbf{p}_1	\mathbf{p}_2	\dots	\mathbf{p}_M	\mathbf{b}_1	\dots	\mathbf{b}_N
\mathbf{p}_1	0	$d(\mathbf{p}_1, \mathbf{p}_2)$	\dots	$d(\mathbf{p}_1, \mathbf{p}_M)$	$d(\mathbf{p}_1, \mathbf{b}_1)$	\dots	$d(\mathbf{p}_1, \mathbf{b}_N)$
\mathbf{p}_2	$d(\mathbf{p}_2, \mathbf{p}_1)$	0	\dots	$d(\mathbf{p}_2, \mathbf{p}_M)$	$d(\mathbf{p}_2, \mathbf{b}_1)$	\dots	$d(\mathbf{p}_2, \mathbf{b}_N)$
\vdots	\vdots	\vdots	\ddots	\vdots	\vdots	\ddots	\vdots
\mathbf{p}_M	$d(\mathbf{p}_M, \mathbf{p}_1)$	$d(\mathbf{p}_M, \mathbf{p}_2)$	\dots	0	$d(\mathbf{p}_M, \mathbf{b}_1)$	\dots	$d(\mathbf{p}_M, \mathbf{b}_N)$
\mathbf{b}_1	$d(\mathbf{b}_1, \mathbf{p}_1)$	$d(\mathbf{b}_1, \mathbf{p}_2)$	\dots	$d(\mathbf{b}_1, \mathbf{p}_M)$	0	\dots	$d(\mathbf{b}_1, \mathbf{b}_N)$
\vdots	\vdots	\vdots	\ddots	\vdots	\vdots	\ddots	\vdots
\mathbf{b}_N	$d(\mathbf{b}_N, \mathbf{p}_1)$	$d(\mathbf{b}_N, \mathbf{p}_2)$	\dots	$d(\mathbf{b}_N, \mathbf{p}_M)$	$d(\mathbf{b}_N, \mathbf{b}_1)$	\dots	0

Table 1. Distance Matrix for Target Points and Regions. **Legend:** Yellow cells () represent point-to-point distances $d(\mathbf{p}_i, \mathbf{p}_j)$, blue cells () represent point-to-region distances $d(\mathbf{p}_i, \mathbf{b}_j)$, and green cells () represent region-to-region distances $d(\mathbf{b}_i, \mathbf{b}_j)$.

3. EXPERIMENTS

3.1 Datasets and experimental setup

Experimental datasets: To validate the effectiveness of the proposed cross-perspective aerial-ground collaborative mapping approach, we conducted experiments using a synthetic dataset. The dataset is a synthetic dataset constructed through manual modeling to create a 3D triangular mesh model representing a scene that includes ground surfaces, vegetation, and building structures. This scene spans an area of $200\text{ m} \times 200\text{ m}$, as shown in Figure 2. To generate a 3D point cloud representation, we sampled the triangular mesh model, treating the resulting point cloud as the *ground-truth* data, and used the Helios LiDAR simulation framework to generate realistic airborne point cloud data, enabling a controlled evaluation of the proposed aerial-ground collaborative mapping framework under various conditions.

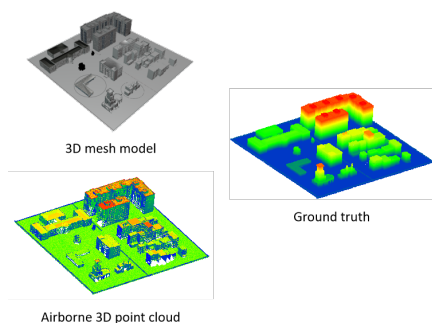


Figure 2. Visualization of dataset.

Experimental platform: To ensure the accurate generation of data supplementation paths, we developed a simulation platform based on Linux and the Robot

Operating System (ROS). This platform integrates the Gazebo open-source simulation tool, which serves as the foundation for creating 3D environments and simulating physical interactions. Building on this, we incorporated CMU’s Autonomous Exploration Development Environment (AEDE) Chao2022, which provides functionalities for motion control, state estimation, autonomous navigation, and high-level planning. These capabilities collectively enable a seamless pipeline for autonomous path planning and execution in simulation environments.

3.2 Experimental Analysis

Results of missing regions: As shown in the figure below, the building missing detection results based on the proposed method are presented. Figure 3(a) displays the generated contours of all buildings along with their skeleton points. It can be observed that the proposed method accurately captures the skeletons of buildings with various shapes. Based on this, missing regions for each building were detected, as shown in Figure 3(b), where the missing region point clouds for each building component are identified. To facilitate a clearer comparison, these missing regions are overlaid with the building components, as shown in Figure 3(c). It is evident that complex buildings tend to have more missing areas, with potential data gaps appearing on multiple walls of the building. In contrast, simple rectangular buildings exhibit fewer missing regions, typically occurring on only one side. This missing data information will serve as an important basis for subsequent data supplementation strategies.

Results of supplementation region: As shown in Figure 4, the data supplementation methods for each building are presented. Based on the terrain data obtained after semantic classification, the traversable node information can be automatically calculated, as shown

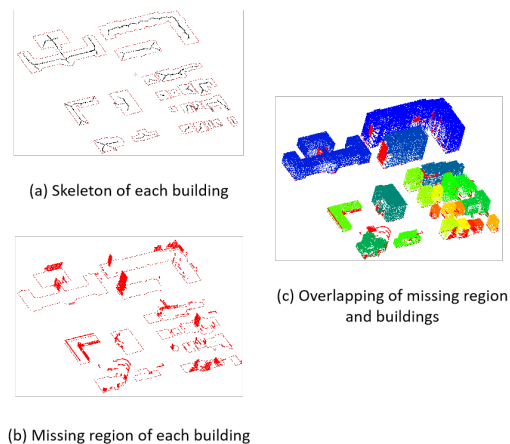


Figure 3. Results of missing regions.

in Figure 4(a). Additionally, based on the proposed method for automatic calculation of point-based and regional-based ground data supplementation and the results of integrity detection, the supplementation strategy for each building is categorized into point-based and region-based methods. For buildings with relatively small missing regions, point-based data collection is primarily employed, whereas for buildings with missing regions exceeding a certain threshold, region-based supplementation is used, as demonstrated in Figures 4(b) and (c).

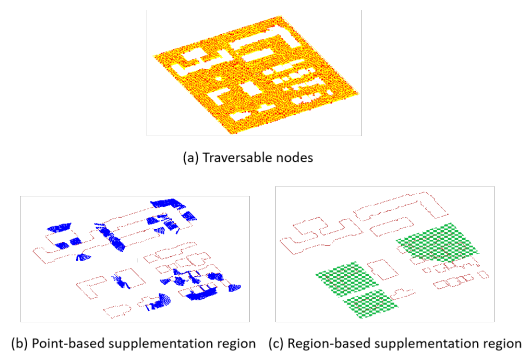


Figure 4. Results of supplementation region.

Optimized results of 3D buildings: To evaluate the effectiveness of the proposed method, extensive experiments were conducted in simulation environments. The evaluation focused on two main aspects: the completeness of the acquired point clouds and the accuracy of the reconstructed building models. The results

in Figure 5 and Table 2 show that the proposed method effectively improves the completeness of building point clouds, increasing the overall point cloud completeness from 83.51% to 89.95%. Additionally, the average distance to the ground truth point cloud is reduced from 0.248m to 0.005m. The results demonstrate that the sky-ground cross-perspective collaborative method significantly enhances point cloud completeness, leading to more detailed and accurate 3D models of buildings. Furthermore, the method outperforms traditional approaches in terms of both data acquisition efficiency and modeling accuracy, making it a promising solution for urban modeling and other applications requiring high-fidelity 3D data. Furthermore, to further assess the effectiveness of the proposed method in improving building modeling results, we employed Polyfit to reconstruct 3D models of the building point clouds before and after data completion and evaluated the corresponding accuracy. As shown in Figure 6, the first building model is relatively complex. Prior to data supplementation, the modeling accuracy of the building's roof was poor; however, after supplementation, the roof structure was modeled more accurately, with the precision improving from 1.7m to 0.189m. After supplementation, the second building's shape closely matches the original point cloud, and the accuracy of the third building was also significantly improved. Therefore, it can be concluded that the proposed method effectively enhances the accuracy of building model reconstruction.

Method	Coverage(%)	Avg dsif	Time Cost (s)
Before Resampling	83.512	0.248	2*29mins
After Resampling	89.952	0.115	

Table 2. Quantitative Results Before and After Resampling

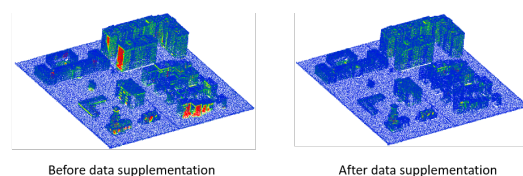


Figure 5. Results of point cloud resampling.

4. ACKNOWLEDGE

This work was supported in part by Natural Science Foundation of China(Project Nos.42471442), Research Project of Natural Science Foundation of Guangdong Province (Project No. 2024A1515030061), Research Project of Shenzhen S and T Innovation Committee

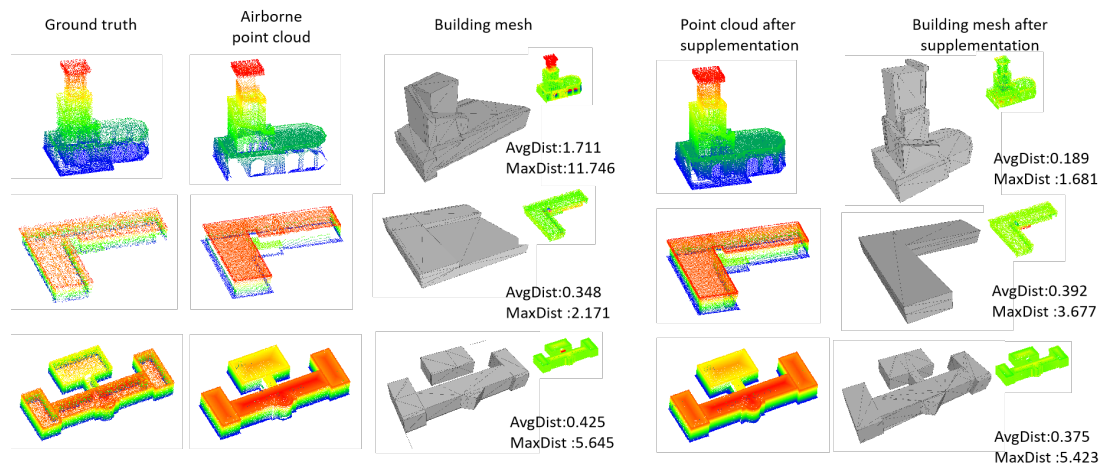


Figure 6. Results of building reconstruction.

(Project No. KJZD20230923115508017) and Research project of State Key Laboratory of Subtropical Building and Urban Science(Project No. 2023ZB18)

REFERENCES

- Cao, Q., Luan, Q., Liu, Y., Wang, R., 2021. The effects of 2D and 3D building morphology on urban environments: A multi-scale analysis in the Beijing metropolitan region. *Building and Environment*, 192, 107635.
- Elhashash, M., Qin, R., 2022. Cross-View SLAM Solver: Global Pose Estimation of Monocular Ground-Level Video Frames for 3D Reconstruction Using a Reference 3D Model from Satellite Images. *ISPRS Journal of Photogrammetry and Remote Sensing*, 188, 62–74.
- Fidan, S., Ulvi, A., Yigit, A. Y., Hamal, S. N. G., Yakar, M., 2023. Combination of Terrestrial Laser Scanning and Unmanned Aerial Vehicle Photogrammetry for Heritage Building Information Modeling: A Case Study of Tarsus St. Paul Church. *Photogrammetric Engineering & Remote Sensing*, 89(12).
- Forster, C., Pizzoli, M., Scaramuzza, D., 2013. Air-ground localization and map augmentation using monocular dense reconstruction. *2013 IEEE/RSJ International Conference on Intelligent Robots and Systems*, IEEE, 3971–3978.
- Fruh, C., Zakhor, A., 2003. Constructing 3D city models by merging aerial and ground views. *IEEE computer graphics and applications*, 23(6), 52–61.
- Huang, X., Zhang, J., Wu, Q., Fan, L., Yuan, C., 2017. A coarse-to-fine algorithm for matching and registration in 3D cross-source point clouds. *IEEE Transactions on Circuits and Systems for Video Technology*, 28(10), 2965–2977.
- Jovanović, D., Milovanov, S., Ruskovski, I., Govedarica, M., Sladić, D., Radulović, A., Pajić, V., 2020. Building virtual 3D city model for smart cities applications: A case study on campus area of the university of novi sad. *ISPRS International Journal of Geo-Information*, 9(8), 476.
- Lee, E., Kwon, Y., Kim, C., Choi, W., Sohn, H.-G., 2024. Multi-source point cloud registration for urban areas using a coarse-to-fine approach. *GIScience & Remote Sensing*, 61(1), 2341557.
- Li, Y., Li, R., Li, Z., Guo, R., Tang, S., 2025. OptiViewNeRF: Optimizing 3D reconstruction via batch view selection and scene uncertainty in Neural Radiance Fields. *International Journal of Applied Earth Observation and Geoinformation*, 136, 104306.
- Li, Z., Shan, J., 2022. RANSAC-based multi primitive building reconstruction from 3D point clouds. *ISPRS Journal of Photogrammetry and Remote Sensing*, 185, 247–260.
- Ling, X., Qin, R., 2022. A Graph-Matching Approach for Cross-View Registration of over-View and Street-View Based Point Clouds. *ISPRS Journal of Photogrammetry and Remote Sensing*, 185, 2–15.
- Liu, J.-k., Qin, R., Arundel, S. T., 2024a. Assessing the Utility of Uncrewed Aerial System Photogrammetric-

- ally Derived Point Clouds for Land Cover Classification in the Alaska North Slope. *Photogrammetric Engineering & Remote Sensing*, 90(7).
- Liu, S., Wang, T., Zhang, Y., Zhou, R., Li, L., Dai, C., Zhang, Y., Wang, L., Wang, H., 2024b. Deep semantic graph matching for large-scale outdoor point cloud registration. *IEEE Transactions on Geoscience and Remote Sensing*.
- Ma, R., Ge, X., Zhu, Q., Jia, X., Jiang, H., Chen, M., Liu, T., 2023. Model-Driven Precise Degradation Analysis Method of Highway Marking Using Mobile Laser Scanning Point Clouds. *Photogrammetric Engineering & Remote Sensing*, 89(4).
- Maboudi, M., Homaei, M., Song, S., Malihi, S., Saadatesherst, M., Gerke, M., 2023. A Review on Viewpoints and Path Planning for UAV-Based 3-D Reconstruction. *IEEE Journal of Selected Topics in Applied Earth Observations and Remote Sensing*, 16, 5026–5048.
- Miller, I. D., Cladera, F., Smith, T., Taylor, C. J., Kumar, V., 2022. Stronger together: Air-ground robotic collaboration using semantics. *IEEE Robotics and Automation Letters*, 7(4), 9643–9650.
- Persad, R. A., Armenakis, C., 2017. Automatic co-registration of 3D multi-sensor point clouds. *ISPRS Journal of Photogrammetry and Remote Sensing*, 130, 162–186.
- Potena, C., Khanna, R., Nieto, J., Siegart, R., Nardi, D., Pretto, A., 2019. AgriColMap: Aerial-ground collaborative 3D mapping for precision farming. *IEEE Robotics and Automation Letters*, 4(2), 1085–1092.
- Sariturk, B., Kumbasar, D., Seker, D. Z., 2023. Comparative Analysis of Different CNN Models for Building Segmentation from Satellite and UAV Images. *Photogrammetric Engineering & Remote Sensing*, 89(2), 97-105.
- Sun, Y., Ye, Y., Kang, J., Fernandez-Beltran, R., Feng, S., Li, X., Luo, C., Zhang, P., Plaza, A., 2023. Cross-View Object Geo-Localization in a Local Region With Satellite Imagery. *IEEE Transactions on Geoscience and Remote Sensing*, 61, 1-16.
- Wu, J., Fu, S., Chen, P., Chen, Q., Pan, X., 2023. Validation of Island 3D-Mapping Based on UAV Spatial Point Cloud Optimization: A Case Study in Dongluo Island of China. *Photogrammetric Engineering & Remote Sensing*, 89(3), 173-182.
- Yu, D., Ji, S., Liu, J., Wei, S., 2021. Automatic 3D building reconstruction from multi-view aerial images with deep learning. *ISPRS Journal of Photogrammetry and Remote Sensing*, 171, 155–170.
- Zhang, W., Qi, J., Wan, P., Wang, H., Xie, D., Wang, X., Yan, G., 2016. An easy-to-use airborne LiDAR data filtering method based on cloth simulation. *Remote sensing*, 8(6), 501.
- Zhou, B., Mo, H., Tang, S., Zhang, X., Li, Q., 2023. Backpack LiDAR-based SLAM with multiple ground constraints for multistory indoor mapping. *IEEE Transactions on Geoscience and Remote Sensing*, 61, 1–16.